

Control-Oriented Flutter/Limit-Cycle-Oscillation Prediction Framework

Darío H. Baldelli*

ZONA Technology, Inc., Scottsdale, Arizona 85258-4578

Richard Lind†

University of Florida, Gainesville, Florida 32611

and

Martin Brenner‡

NASA Dryden Flight Research Center, Edwards Air Force Base, California 93253

DOI: 10.2514/1.36117

In this work, an aeroelastic prediction framework is formulated by blending control-oriented techniques that consist of linear fractional transformation representation, identification of nonlinear operators, and stability boundary prediction for both flutter and limit-cycle-oscillation phenomena. The final product is an efficient tool devised to identify, characterize, and predict flutter/limit-cycle-oscillation conditions by taking full advantage of the information embedded in the flight data. A novel data-based amplitude- and airspeed-dependent operator is developed to consistently fit within the μ -analysis framework. By exploiting the algebraic structure of the identified block-oriented models, a parameter-varying model is devised to represent its amplitude- and airspeed-dependent dynamic behavior. To illustrate this flutter/limit-cycle-oscillation prediction framework, the developed algorithms are applied to a structurally nonlinear two-dimensional wing section while including uncertain stiffness parameters.

I. Introduction

A NOVEL control-oriented flutter/limit-cycle-oscillation (LCO) prediction tool using aeroelastic modeling enhancement techniques to assist in flight-testing for envelope-expansion purposes is presented. It is well known that the addition and/or modification of external equipment and stores on the aircraft deeply impact its aeroelastic characteristics, which are not fully predictable using linear flutter engineering tools [1,2]. These configurations arise frequently on military fighters with stores such as fuel pods and weapons but are also present on transports that have engine nacelles. The common approach for envelope expansion is to take the aircraft to a stabilized test point and measure vibration data. Flight-test data from the test points are analyzed to predict the speed at which the onset of flutter/LCO may be encountered. The envelope is expanded by increasing the airspeed at successive test points until the data analysis indicates that the aeroelastic instability speed is close within a certain safety margin. The proposed control-oriented framework is devised to naturally fit within this standard certification procedure.

During the past years, several modeling hypotheses have been proposed as the representative model for LCO of aircraft/wings [3]. Among other modeling approaches, there are the aerodynamic-driven models due to various agents such as vortex dynamics, transonic shock with/without flow separation [4], the structural-based models due to nonlinear stiffness [5], nonlinear friction damping [6], actuation-related model [7], the internal resonance model [8,9], etc.

In contrast to the current prevailing LCO prediction methodologies that mostly adopt high-level computational fluid dynamics methods with built-in nonlinear models, the proposed framework approaches the flutter and/or LCO characterization and prediction

problem from an entirely different perspective. An aeroelastic prediction framework is formulated by blending control-oriented techniques that consist of linear fractional transformation (LFT) representation, identification of nonlinear operators, and stability boundary prediction for both flutter and LCO phenomena. The final product is an efficient tool devised to identify, characterize, and predict flutter/LCO conditions by taking full advantage of the information embedded in the flight data.

A quasi-linear data-based amplitude- and airspeed-dependent operator is developed to consistently fit within the μ -analysis framework. By exploiting the algebraic structure of the identified set of nonlinear block-oriented models, a parameter-varying model is devised to represent its amplitude- and airspeed-dependent dynamic behavior. The underlying concept seeks to properly incorporate the influence of varying flight conditions on the aeroelastic dynamics of the aircraft. Clearly, by fixing the nonlinearity amplitude/strength, the inclusion of airspeed dependency simplifies the task of predicting the onset of aeroelastic instabilities.

The outline of the paper is as follows. In Sec. II, the general formulation for the flutter/LCO prediction framework is described. It includes how to model and parameterize an uncertain aeroelastic system, how to estimate and build parameter-varying unknown-dynamics operator, and how to transform the match-point solution setup into a linear/quasi-linear framework to accurately predict flutter/LCO instabilities. Finally, in Sec. III, promising results are obtained when this control-oriented flutter/LCO prediction approach is applied to noisy input–output simulated measurements from a structurally nonlinear prototypical two-dimensional wing section. Comments are provided concerning possible advantages and limitations of the proposed methodology.

II. Flutter/LCO Prediction Tool: General Formulation

Currently, no immediate modeling approach is readily available to fully describe actual nonlinear aeroelastic dynamic systems. Hence, the proposed approach for formulating a flutter/LCO predictor is to augment the current μ -analysis approach [10] with a set of flight-data-based nonlinear operators [11]. This concept involves a representation of the aeroelastic dynamics that includes both linear and nonlinear components. Stability margins would then be computed that indicate the flight conditions associated with linear

Received 13 December 2007; revision received 17 May 2008; accepted for publication 22 May 2008. Copyright © 2008 by Darío H. Baldelli. Published by the American Institute of Aeronautics and Astronautics, Inc., with permission. Copies of this paper may be made for personal or internal use, on condition that the copier pay the \$10.00 per-copy fee to the Copyright Clearance Center, Inc., 222 Rosewood Drive, Danvers, MA 01923; include the code 0731-5090/08 \$10.00 in correspondence with the CCC.

*9489 East Ironwood Square Drive; dario@zonatech.com.

†Department of Mechanical and Aerospace Engineering; ricklind@ufl.edu.

‡Aerostructures Branch; martin.brenner@dfrc.nasa.gov.

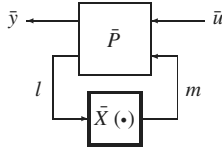


Fig. 1 Generic nonlinear feedback framework.

and nonlinear aeroelastic instabilities. To this end, a general aeroelastic model enhancement feedback setup using nonlinear identification techniques was devised [12,13].

Specific formulations were derived for two different unmodeled dynamic identification scenarios. One scenario assumes that the unknown dynamics are purely a function of the measured states $\bar{X}(l) = \bar{X}(x)$, whereas the other assumes that the unknown dynamics are purely a function of the measurement inputs $\bar{X}(l) = \bar{X}(u)$. In both, nonlinear block-oriented system identification techniques can be employed to estimate the unmodeled dynamic operator $X(\cdot)$ using a discrete set of stabilized test points.

As schematically shown in Fig. 1, this model can now be represented as a nonlinear feedback interconnection:

$$\bar{y} = F_l[\bar{P}, \bar{X}(l)]\bar{u} \quad (1)$$

$$\bar{P} = \begin{bmatrix} P_{11} & P_{12} \\ P_{21} & P_{22} \end{bmatrix} \quad (2)$$

where \bar{P} is the nominal plant, and P_{jk} ($j, k = 1, 2$) are the transfer functions related to the input $\{\bar{u}^T \ m^T\}^T$ and output $\{\bar{y}^T \ l^T\}^T$ signals. Note that the known and unknown elements of the model are related by the signal $m = \bar{X}(l)$. Here, the signal l is measured and can be inferred from the knowledge of the measured input \bar{u} or output \bar{y} signals, respectively.

In [14], it was shown how the inclusion of parameter dependency simplifies the task of predicting the onset of aeroelastic instabilities. That approach is further extended here, where the analysis is sought to iterate over the airspeed by considering the single model resulting by blending the known dynamics \bar{P}_i and the data-based parameter-dependent unmodeled dynamics \bar{X}_i ($i = 1, \dots, n_{tp}$, with n_{tp} being the number of stabilized test points). Note that both operators are devised to be parameterized around the airspeed and the coupling process is performed using LFT algebra [15]. Both operators are now conveniently parameterized around the airspeed at the i th flight condition by introducing a perturbation δ_v^i to the nominal airspeed V_0 , such that $V^i = V_0 + \delta_v^i$.

In Fig. 2 the known dynamics \bar{P}_i are described by an upper LFT defined between the nominal aeroelastic plant P parameterized around the airspeed perturbation parameter δ_v^i , as

$$\begin{Bmatrix} \bar{y} \\ l \end{Bmatrix} = \underbrace{F_u[P, \delta_v^i]}_{\bar{P}_i} \begin{Bmatrix} \bar{u} \\ m \end{Bmatrix} \quad (3)$$

and the unknown dynamics $\bar{X}_i(\cdot)$ are described using a lower LFT: that is,

$$m = \underbrace{F_l[X, \delta_v^i]}_{\bar{X}_i(\cdot)} l \quad (4)$$

It is conjectured that at the i th flight-test point ($i = 1, \dots, n_{tp}$) of the unmodeled dynamic system $\bar{X}_i(x)$ will give rise to a nonlinear operator that can be replaced with a block-oriented model such as the Hammerstein model $\bar{X}_i(x) = G_X^i \gamma_i(x)$ or the Wiener model $\gamma_i(v)$ with the signal $v = G_X^i x$.

A. Aeroelastic Modeling for Robust Flutter/LCO Prediction

One of the objectives of this research work was to represent an aeroelastic model using a LFT setup for the most general aeroelastic systems defined using linear flutter engineering tools. The associated

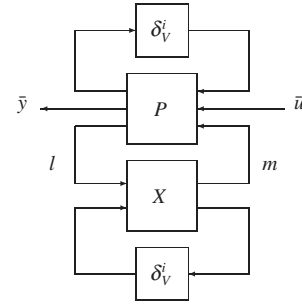


Fig. 2 Feedback relationship of operators.

model will contain information on the structural model, including the control effectors' inertial coupling, the unsteady aerodynamic rational function approximation, and the interconnection structure and/or exogenous signals, among others [13,16].

The modeling process starts with the aeroelastic equations of motion of the nominal aeroelastic system written in the time domain:

$$[M_s \ M_c] \begin{Bmatrix} \ddot{\eta} \\ \dot{\delta}_c \end{Bmatrix} + C_s \dot{\eta} + K_s \eta + X(l) = -\bar{q} [Q_s \ Q_c] \begin{Bmatrix} \eta \\ \delta_c \end{Bmatrix} \quad (5)$$

where $M_s \in \mathbb{R}^{n_s \times n_s}$, $C_s \in \mathbb{R}^{n_s \times n_s}$, and $K_s \in \mathbb{R}^{n_s \times n_s}$ are the generalized mass, damping, and stiffness structural matrices; $M_c \in \mathbb{R}^{n_s \times n_c}$ is the inertial coupling mass matrix related with the control surfaces set; $\eta \in \mathbb{R}^{n_s}$ is the vector of generalized coordinates; $\delta_c \in \mathbb{R}^{n_c}$ is the vector of control effector states; and, as before, $X(l)$ is the unmodeled dynamics operator as a function of the signal l to be defined. In addition, the aerodynamic force coefficient matrix $Q(p)$ is explicitly defined in terms of the η and δ_c vectors as

$$[Q_s(p) \ Q_c(p)] \begin{Bmatrix} \eta \\ \delta_c \end{Bmatrix} = [A_{s_0} \ A_{c_0}] \begin{Bmatrix} \eta \\ \delta_c \end{Bmatrix} + [A_{s_1} \ A_{c_1}] \begin{Bmatrix} \dot{\eta} \\ \dot{\delta}_c \end{Bmatrix} + [A_{s_2} \ A_{c_2}] \begin{Bmatrix} \ddot{\eta} \\ \ddot{\delta}_c \end{Bmatrix} + \quad (6)$$

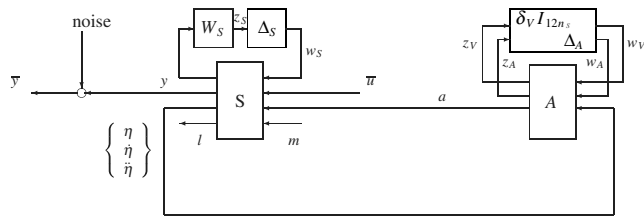
$$D(Ip - R)^{-1} [E_s \ E_c] \begin{Bmatrix} \dot{\eta} \\ \dot{\delta}_c \end{Bmatrix} \quad (7)$$

where A_{ij} and E_i with $i = s$ or c and $j = 0, 1, 2$, are column-partitioned matrices in accordance with the number of structural elastic modes n_s and control effectors n_c , respectively. Here, p is the nondimensional complex Laplace variable $p = sL/V$, where L is the reference length and all the coefficient matrices are real ones.

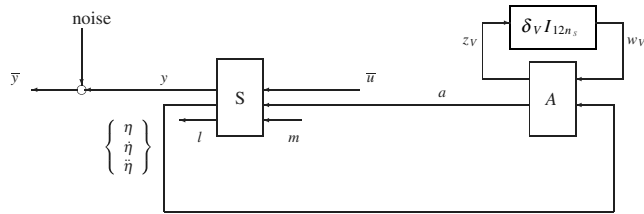
Because the aerodynamic data are given for harmonic oscillations, to allow for time simulations, the aerodynamic loads are first approximated in the Laplace domain using a rational function approximation technique [17,18]. The approximation process involves the replacement of p by ik , where k is the nondimensional frequency $\omega L/V$, with ω being the frequency of oscillation. Then least-squares procedures are used to compute the matrices approximation coefficients A_{ij} , D , E_j , and R . Here, the A_{ij} with $i = s$ or c and $j = 0, 1, 2$ coefficient matrices represent the quasi-steady aerodynamic forces, as an equivalent aerodynamic stiffness, aerodynamic damping, and aerodynamic inertia, whereas the remnant terms are used to model the flow unsteadiness by the Padé approximants.

For robustness analysis purposes, uncertain and/or unmodeled operators are being incorporated in the aeroelastic system, and the equation of motion is broken down into several LFT subsystems. The proposed uncertain aeroelastic system in LFT form is depicted in Fig. 3a.

The structural dynamics can be represented by the linear matrix coefficients S and the uncertainty block Δ_s . In a similar way, the unsteady aerodynamic loads are described by the linear element A , a parametric uncertainty around the airspeed perturbation parameter,



a) Uncertain aeroelastic model



b) Nominal aeroelastic model

Fig. 3 Generic aeroelastic model built by LFT operators for model-updating purposes.

δ_V , as well as the uncertainty block Δ_A associated with the lag terms contained in the matrix R . Hence, the LFT framework will allow the analysis of the linear components with uncertain and nonlinear operators. This analysis is actually simplified using LFT algebra as follows:

1) The nominal linear model, obtained by LFT algebra between S and A ($\Delta_S = \Delta_A = X(\cdot) \equiv 0$), can be analyzed by itself to determine a traditional flutter margin.

2) The open-loop linear elements S , A , Δ_S , and Δ_A can be analyzed to determine a robust flutter margin.

3) The nonlinearity can be included such that analyzing the LFT interconnection of S , A , Δ_S , Δ_A , and $X(\cdot)$, admits stability margins for limit cycle oscillations with or without uncertainties.

Also, any of these analyses can be augmented for aeroservoelasticity purposes by including the actuator dynamics as well as the flight controller. Note that an example of this approach has been published [11] in which a typical airfoil section including control-surface free play was considered. The nonlinear operator was identified using a set of input/output (I/O) wind-tunnel test data and the traditional flutter margin, robust flutter margin, and nominal and robust LCO boundaries were computed for a single wind-tunnel test point. In this work, we are extending the flutter/LCO detection framework by considering the influence of the nonlinear amplitude strength as well as varying flight conditions on the unmodeled dynamics operator $\bar{X}_i(\cdot)$ ($i = 1, \dots, n_{tp}$).

In what follows, the nominal aeroelastic model depicted in Fig. 3b is obtained by LFT algebra between the nominal S and A operators (i.e., $\Delta_S = \Delta_A \equiv 0$). It is used to determine a traditional flutter margin within the proposed model-updating procedure. In this way, the resulting aeroelastic model will be a function of a single parameter δ_V to describe the flight condition dependency [13,14].

B. Unknown Dynamics Operator Representation by Block-Oriented Models

In this section, it is proposed to employ block-oriented models to augment linear aeroelastic models [19] with nonlinear operators derived by analyzing wind-tunnel or flight-test data. Hence, two paradigms are proposed to represent as well as to identify the nonlinear behavior embedded in the unmodeled dynamics data. These paradigms are based on the concepts of Hammerstein and Wiener models [20,21], as depicted in Figs. 4a and 4b. Both of these can represent nonlinearities; however, each has a fundamentally different nature. A Hammerstein model identification approach is applied when measurements at the input of the unknown nonlinear map are accessible, otherwise, a Wiener method is suggested (sensor nonlinearity). Clearly, this topology represents a first attempt to

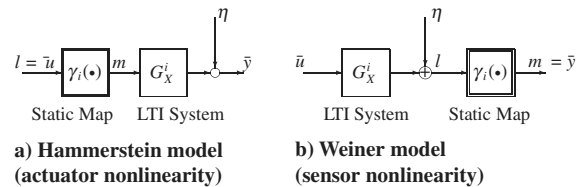


Fig. 4 Block-oriented nonlinear models.

extend the linear models realm in order to represent nonlinear dynamic processes.

Several appealing features can be mentioned when using block-oriented models. Among them, it can be cited that it is easy to incorporate a priori knowledge on the system, and they represent a low-cost solution in terms of identification and control computations [22].

The underlying structure of a generic block-oriented model assumes that the steady-state behavior is determined by the static nonlinearity, whereas the dynamic behavior is determined together with the static map and the linear-time-invariant (LTI) part. The model consists of a nonlinearity $\gamma_i(\cdot)$ in series connection with a LTI system described by its transfer function matrix G_X^i ; that is,

$$G_X^i(q) = \sum_{l=0}^{p-1} b_l B_l(q), \quad \gamma_i(\cdot) = \sum_{i=1}^r \alpha_i g_i(\cdot) \quad (8)$$

where $g_i(\cdot): \mathbf{R}^n \rightarrow \mathbf{R}^n$ are known vector fields, $\alpha_i \in \mathbf{R}^{n \times n}$, ($i = 1, \dots, r$) are vector parameters, $G_X^i(q) \in \mathbf{H}_2^{m \times n}$, $b_l \in \mathbf{R}^{m \times n}$, and q is the forward-shift operator.

To allow an accurate matching with the unmodeled dynamics data, the block-oriented models use an a priori set of orthonormal bases, $\{B_l(q)\}_{l=0}^{p-1}$, tuned with linear modal information extracted from an N point data set, $\{u_k, y_k\}_{k=1}^N$. To this end, the orthonormal bases set will be generated using the cascade of input-normal balanced state-space realizations of two-parameters Kautz filters [23]. In a subsequent step, the discrete-time transfer function matrix $G_X^i(q)$ is converted to its continuous-time counterpart $G_X^i(s)$, where s stands for the Laplace variable.

Note that the nonlinear behavior given by the block-oriented operator will have a global or local character, depending on the available information of the nonlinear phenomena under investigation. For example, if the user is able to properly isolate a set of I/O signals related with a structural nonlinearity, then the identified static map will not change under different flight conditions, providing a global character. On the contrary, if she/he is able to collect I/O data related with nonlinear aerodynamic behavior, such as those represented by transonic shock waves with or without flow separation, the resulting static map will presumably be flight-condition-dependent and local in nature.

Based on these assumptions, it is conjectured that the method could be able to identify the origin or character of the nonlinear behavior embedded in the flight-test data if informative-enough experimental evidence is recorded during the data-gathering process. From the flight-test engineer's point of view, given the generally poor quality of the aeroelastic responses recorded during flutter clearance programs as well as the possible unobserved dynamics due to the reduced number of sensors that have been installed on the aircraft, it could be very challenging to obtain informative-enough I/O data to correctly characterize the underlying nonlinear phenomena. However, the proposed flutter/LCO detection framework is formulated to deal with both identification scenarios if a block-oriented model is estimated at each flight-test point.

C. Block-Oriented Parameter-Varying Model

The identification of the unknown dynamics operator $\bar{X}_i(\cdot)$ is further extended to include dependency on the main parameters affecting the nonlinear dynamics: in particular, dependency on flight conditions as well as on the input signal strength to the identified nonlinear operator. As a result, airspeed $\bar{X}_i(\delta_V)$ as well as

amplitude- and airspeed-dependent $\bar{X}_i(a, \delta_v^i)$ operators based on block-oriented models are successfully formulated and synthesized. The airspeed dependency is computed by fitting the coefficients of the identified LTI part $G_X^i(s)$ to a quadratic matrix polynomial function of the airspeed; that is,

$$\underbrace{\begin{bmatrix} A^i & B^i \\ C^i & D^i \end{bmatrix}}_{G_X^i(s)} \simeq \begin{bmatrix} \hat{A}(V^i) & \hat{B}(V^i) \\ \hat{C}(V^i) & \hat{D}(V^i) \end{bmatrix} \quad (9)$$

$$G_X^i(s) = \begin{bmatrix} A_0 + A_1 V^i + A_2 (V^i)^2 & B_0 + B_1 V^i + B_2 (V^i)^2 \\ C_0 + C_1 V^i + C_2 (V^i)^2 & D_0 + D_1 V^i + D_2 (V^i)^2 \end{bmatrix} \quad (10)$$

Equation (10) results in a form that can easily be parameterized around an airspeed perturbation parameter δ_v^i , such that [16]

$$V^i = V_0 + \delta_v^i \quad (11)$$

where V_0 is the i th flight-test point's airspeed value. Clearly, this transformation allows the operator $G_X^i(s)$ to be sought as a parameter-varying system expressed as a lower LFT system:

$$G_X^i(s) = F_l[G_X(V_0), \delta_v^i] \quad (12)$$

where the resulting linear operator $G_X(V_0)$ is a function of the nominal waypoint airspeed V_0 .

Additionally, the amplitude dependency is included by replacing the static map $\gamma_i(\cdot)$ operator by its sinusoidal input describing function $N_i(a)$ [24]. The strength a of the input signal to the operator $N_i(a)$ becomes the amplitude-dependent parameter in this unique formulation. Figure 5 schematically depicts the devised Hammerstein-based amplitude- and airspeed-dependent operator $X_i^H(a, \delta_v^i)$. In a similar way, a Wiener-based amplitude- and airspeed-dependent operator $X_i^W(a, \delta_v^i)$ can be generated if required. To improve its prediction capabilities, the parameter-varying model $X_i^H(a, \delta_v^i)$ [$X_i^W(a, \delta_v^i)$] will be estimated based on the least-squares fit of the data recorded up to the actual nominal waypoint's airspeed value [14].

D. Robust Flutter/LCO Predictor Engine Formulation

Figure 6 schematically shows the devised flutter/LCO predictor engine as a combination of the nominal aeroelastic model P (see Fig. 2) parameterized around the airspeed parameter δ_v^i , together with the unknown dynamic operator $\bar{X}_i^H(a, \delta_v^i)$ generated from a set of identified Hammerstein models at different airspeeds (i.e., $\{\gamma_i(\cdot), G_X^i\}_{i=1}^{n_{wp}}$ with $G_X^i = F_l[G_X(V_0), \delta_v^i]$).

A generalized condition of oscillation for this quasi-linear aeroelastic model is now proposed to accurately predict the flutter/LCO phenomena. In Fig. 6, the block R_i^H is obtained by combining the linear elements P and $G_X(V_0)$ using suitable LFT algebra (i.e., $R_i^H = F_l[P, G_X(V_0)]$). As in the previous section, a Wiener-based operator R_i^W can be achieved.

The necessary condition for the existence of flutter/LCO is obtained as [25,26]

$$\det(I - F_l[R_i^H, N_i(a)], \delta_v^i I_{PX}) = 0 \quad (13)$$

Specifically, by fixing $N_i(a)$, a new linear operator is computed as $M_i^H = F_l[R_i^H, N_i(a)]$ ($M_i^W = F_l[R_i^W, N_i(a)]$). Then, by varying the airspeed parameter δ_v^i , the least damped eigenvalues of M_i^H (M_i^W) are driven to the imaginary axis, and the flutter/LCO boundaries are efficiently computed. The μ -analysis framework is used here to detect flutter/LCO boundaries by computing the singularity of M_i^H (M_i^W) as a function of the parameter uncertainty $\delta_v^i I_{PX}$.

After collecting aeroelastic response data from a set of stable and safe waypoints, either an airspeed-dependent operator $X_i^H(\delta_v^i)$ [$X_i^W(\delta_v^i)$] or an amplitude- and airspeed-dependent operator $X_i^H(a, \delta_v^i)$ [$X_i^W(a, \delta_v^i)$] can be generated. In the former case, the flutter speed and frequency is found by increasing the value of δ_v^i

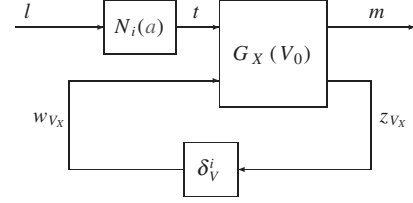


Fig. 5 Hammerstein-based amplitude- and airspeed-dependent operator $X_i^H(a, \delta_v^i)$.

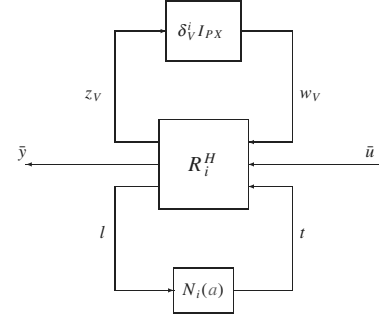


Fig. 6 Hammerstein-based flutter/LCO predictor block diagram.

until the least damped eigenvalue of the operator R_i^H (R_i^W) has a positive real part and the system become unstable. In the latter case, for each value of the amplitude parameter a , a new operator M_i^H (M_i^W) is computed, and as in the previous case, the value of δ_v^i is increased until its least damped eigenvalue has a positive real part. In this way, by fixing the $N(a)_i$, the LCO boundary can be efficiently detected. As the waypoint airspeed is further increased during the flight expansion program, at a certain airspeed $V_0 = V^*$, a value of the amplitude parameter a will be reached ($a = a^*$) at which the operator $M_i^H = F_l[R_i^H, N_i(a^*)]$ will already have its least damped eigenvalues located at the imaginary axis, even for $\delta_v^i = 0$. Therefore, the related LCO parameters will be defined as $V_{LCO} = V^*$ and $a_{LCO} = a^*$, respectively.

In other words, by updating an accurate linear aeroelastic model P using engineering aeroelastic models [19] with the unknown dynamic operator shown in Fig. 5, $\bar{X}_i^H(a, \delta_v^i)$, identified using data collected at several safe and stable waypoints, the proposed flutter/LCO engine can become a very useful tool within the control room to help the flight-test engineer to predict the flutter/LCO instability boundaries in real time.

III. Application Example: Flutter/LCO Prediction of an Aeroelastic System

The selected case is a structurally nonlinear prototypical two-dimensional wing section. The nonlinearity included in the model is a memoryless quintic gain affecting the stiffness of the pitch motion through the pitch rotation of the airfoil, (k_{α^5}). Note that only the order of the actual experimental nonlinearity is used, not the actual estimated coefficients as reported in [27].

Figure 7 shows the simulation setup to generate the linear/nonlinear pitch angle signal $\bar{y}_k \equiv \alpha_k$ as well as other responses from the linear model. The simulated measured system output is the pitch angle α_k , which is corrupted with a zero-mean Gaussian distributed white noise with a variable standard deviation σ , whereas the system input is the flap deflection β_k . A chirp signal is commanded to the flap to generate responses from the simulation. This chirp command ranges from 0.0 to 2.5 Hz over 32 s. The magnitude of this flap command is 10 deg.

In what follows, the *unknown dynamics* signal e_k is defined as the difference between the measured signal \bar{y}_k (linear/nonlinear dynamics) and the simulated linear part of the model, $y_k = P_{11}\bar{u}_k$. It is then proposed that a Hammerstein model structure can identify the unmodeled dynamics from N point data of the error signal e_k .

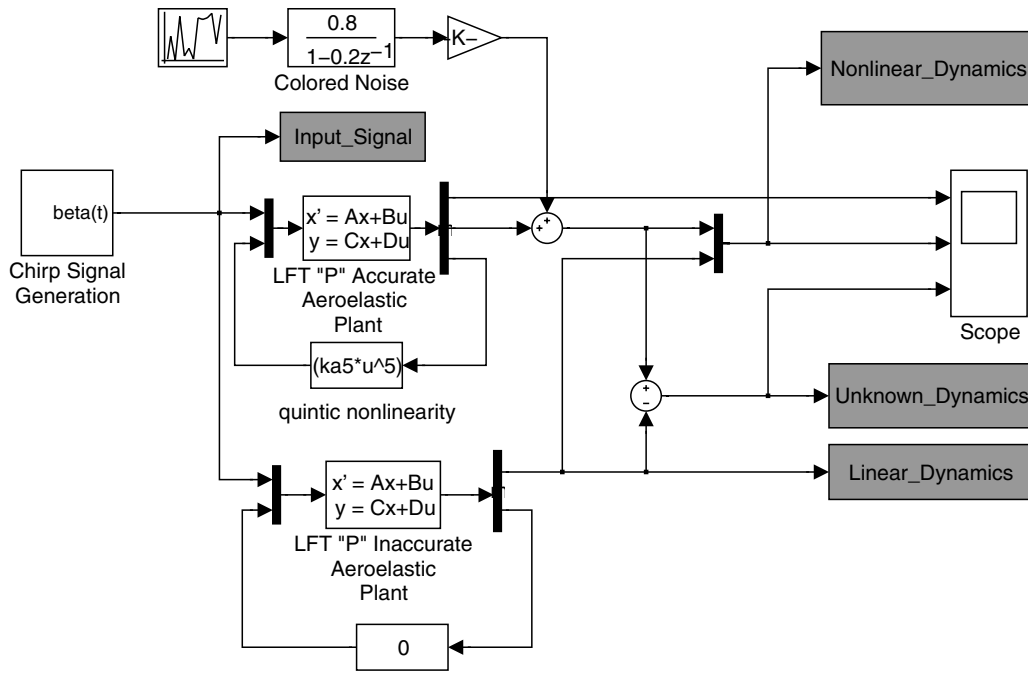


Fig. 7 Simulation setup for input/output signals generation.

In connection with the linear portion of the model, an explicit modeling error is incorporated by an inaccurate value of the pitch stiffness k_α . Therefore, an accurate linear model results when the nominal pitch stiffness equal to $k_\alpha = 2.82$ Nm/rad is used, whereas the inaccurate linear model is defined by $k_\alpha = 2.26$ Nm/rad. This represents a 20% reduction (uncertainty) of the nominal pitch stiffness value. The geometry and main parameters to be used in the numerical simulations are those noted in Table 1 [27].

It is noted that by assuming a structural nonlinearity, the problem is simplified, given that the identified static map is shown to be invariant with respect to the airspeed. Hence, only the LTI part of the block-oriented model is transformed into a parameter-varying model throughout the airspeed parameterization process described in Sec. II.C. The basic representation of the pitch-plunge aeroelastic system under consideration is given by

$$M\ddot{\eta} + C\dot{\eta} + K\eta + X(l) = V^2D\eta + VE\dot{\eta} + V^2F\beta \quad (14)$$

where

Table 1 Pitch-plunge system parameters

Geometric parameters	
Semichord b	0.135 m
Elastic axis e	-0.6
Mass parameters	
Mass, m	12.387 kg
Inertial parameters	
x_α	0.2466
I_α	0.065 kg m ²
Damping parameters	
c_h	27.43 kg/s
c_α	0.180 kg m ² /s
Stiffness parameters	
k_h	2844.2 N/m
k_α	2.82 Nm/rad
k_{α^5}	70 Nm/rad
Aerodynamics parameters	
c_{l_α}	2π
c_{l_β}	3.358
c_{m_α}	-0.628
c_{m_β}	-0.635

$$M = \begin{bmatrix} m & mx_\alpha b \\ mx_\alpha b & I_\alpha \end{bmatrix}, \quad C = \begin{bmatrix} c_h & 0 \\ 0 & c_\alpha \end{bmatrix}$$

$$K = \begin{bmatrix} k_h & 0 \\ 0 & k_\alpha \end{bmatrix}, \quad D = \begin{bmatrix} 0 & -c_{l_\alpha} \rho b \\ 0 & c_{m_\alpha} \rho b^2 \end{bmatrix}$$

$$E = \begin{bmatrix} -c_{l_\alpha} \rho b & -c_{l_\alpha} \rho b^2 (0.5 - e) \\ c_{m_\alpha} \rho b^2 & c_{m_\alpha} \rho b^3 (0.5 - e) \end{bmatrix}, \quad F = \begin{bmatrix} -c_{l_\beta} \rho b \\ c_{m_\beta} \rho b^2 \end{bmatrix} \quad (15)$$

where the vector η is defined as $\eta = [h \ \alpha]^T$. The function $X(l)$ represents an unknown, possibly nonlinear, contribution to the dynamics. The dynamics in Eq. (14) can be reformulated in a form that includes feedback relationships between the known dynamics and the unknown dynamics along with a perturbation to airspeed. As mentioned in Sec. II, the airspeed is replaced with a nominal value plus a perturbation parameter (i.e., $V^i = V_0 + \delta_V^i$). These definitions allow Eq. (14) to be written as Eq. (16):

$$\ddot{\eta} = M^{-1}[(V_0^2 D - K)\eta + (V_0 E - C)\dot{\eta} + V_0^2 F\beta - w_l + w_1 + w_3] \quad (16)$$

The derivation of the required expression is accomplished by introducing the set of signals defined in Eq. (17):

$$l = \eta, \quad w_l = X(l)$$

$$z_1 = 2V_0 D\eta + E\dot{\eta} + 2V_0 F\beta, \quad w_1 = \delta_V^i z_1$$

$$z_2 = D\eta + F\beta, \quad w_2 = \delta_V^i z_2$$

$$z_3 = w_2, \quad w_3 = \delta_V^i z_3 \quad (17)$$

The nominal LFT aeroelastic model P is expressed in state-space form in Eq. (18) [14]:

$$\begin{bmatrix} \dot{\eta} \\ \ddot{\eta} \\ z_1 \\ z_2 \\ z_3 \\ y \\ l \end{bmatrix} = \begin{bmatrix} A_P & B_P \\ C_P & D_P \end{bmatrix} \begin{bmatrix} \eta \\ \dot{\eta} \\ w_1 \\ w_2 \\ w_3 \\ \beta \\ w_l \end{bmatrix} \quad (18)$$

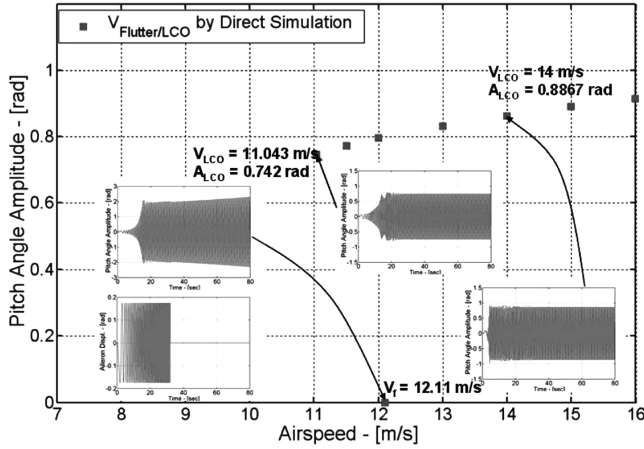


Fig. 8 Simulated flutter/LCO boundary, (noisy case).

with the quadruple matrices (A_P , B_P , C_P , and D_P) defined as

$$A_P = \begin{bmatrix} 0 & I \\ M^{-1}(V_0^2 D - K) & M^{-1}(V_0 E - C) \end{bmatrix}$$

$$B_P = \begin{bmatrix} [0 \ 0 \ 0] & 0 & 0 \\ [M^{-1} \ 0 \ M^{-1}] & M^{-1} V_0^2 F & -M^{-1} t_\alpha^T \end{bmatrix}$$

$$C_P = \begin{bmatrix} [2V_0 D] & [E] \\ D & 0 \\ 0 & 0 \\ I & 0 \\ t_\alpha & 0 \end{bmatrix}$$

$$D_P = \begin{bmatrix} [0 \ 0 \ 0] & [2V_0 F] & [0] \\ [0 \ 0 \ 0] & F & [0] \\ [0 \ I \ 0] & 0 & [0] \\ [0 \ 0 \ 0] & 0 & [0] \\ [0 \ 0 \ 0] & 0 & [0] \end{bmatrix}$$

and the vector $t_\alpha = [0 \ 1]$ selects the pitch angle variable (i.e., $l = t_\alpha \eta = \alpha$).

A. Linear and Nonlinear Instability Boundaries: Direct Simulation Results

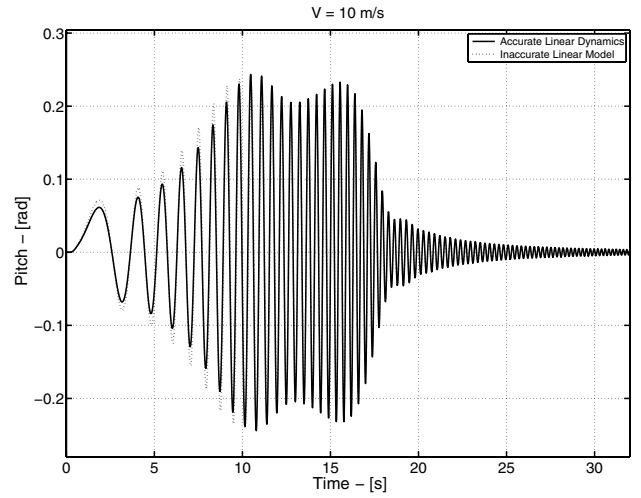
The linear and nonlinear instability boundaries for this case study are computed by switching off/on the actual quintic nonlinearity using a fixed-step-size numerical integration scheme implemented in Simulink (Dormand–Prince) [28]. The qualitative and quantitative changes are depicted in Fig. 8. It shows only a measure of the magnitude (or norm) of an equilibrium point or limit cycle of the nonlinear aeroelastic system [3].

On the same plot, the time traces of both the aileron deflection excitation signal (chirp) $\beta(t)$ and the pitch angle $\bar{y}(t) = \alpha(t)$ are included. It can be observed that the divergent as well as the constant oscillatory behaviors related with the flutter and LCO phenomena are present.

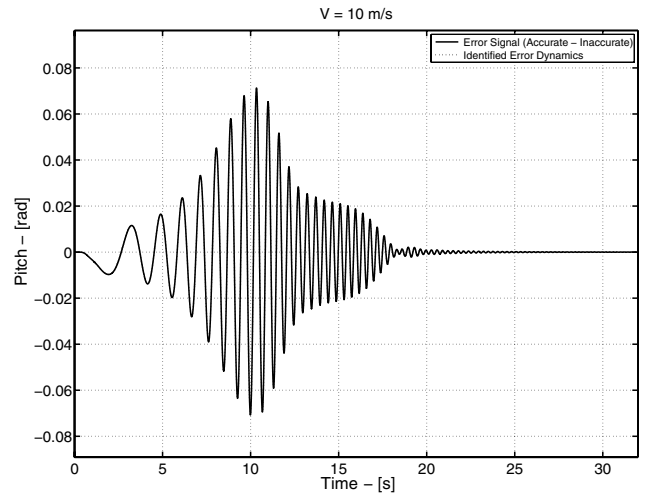
Table 2 Simulated flutter/LCO boundary summary, (noise case)

Airspeed, m/s	Flutter/LCO	LCO amp., rad
12.11	FLT	—
10.56	LCO	0.72
11.04	LCO	0.76
12.00	LCO	0.82
13.00	LCO	0.85
14.00	LCO	0.88
15.00	LCO	0.91
16.00	LCO	0.94

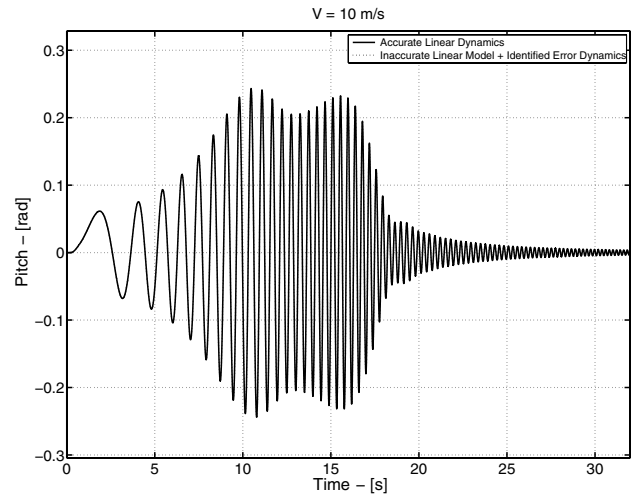
Technically, by switching off the quintic nonlinearity, the flutter instability point is obtained when the speed achieves a value $V_f = 12.11$ m/s. On the contrary, when the nonlinearity is present, a presumably subcritical bifurcation LCO phenomenon arises. The



a) Linear dynamics response \bar{y}_k and inaccurate linear model y_k



b) Measured unknown dynamics e_k and estimated unknown dynamics \hat{e}_k



c) Linear dynamics response \bar{y}_k and updated model response $y_k + \hat{e}_k$

Fig. 9 Measured and simulated pitch angle response to a chirp input at $V_0 = 12$ m/s.

Table 3 Predicted flutter boundary summary

Model	Flutter speed, m/s	Flutter freq., Hz
True	12.11	2.11
$F_u[P, \delta_v^i]$	12.38	2.08
$F_u[R_7, \delta_v^i]$	12.31	2.09
$F_u[R_8, \delta_v^i]$	12.29	2.09
$F_u[R_9, \delta_v^i]$	12.28	2.09
$F_u[R_{10}, \delta_v^i]$	12.27	2.09
$F_u[R_{11}, \delta_v^i]$	12.23	2.09
$F_u[R_{12}, \delta_v^i]$	12.13	2.10

so-called saddle-node point is achieved at $V_{LCO} = 10.561$ m/s with a pitch amplitude of $\alpha_{LCO} = 0.6979$ rad.

In what follows, the general formulation laid out in Sec. II.D will be employed to predict the flutter/LCO boundaries, and those results will be compared with the results depicted in Fig. 8. Additionally, Table 2 indicates the associated flutter/LCO coordinates represented by the square points in Fig. 8.

B. Linear Prediction Case-Flutter

Responses of the aeroelastic pitch-plunge dynamics are simulated to illustrate the differences between the true system and the assumed model. The known dynamics operator P is built using the inaccurate

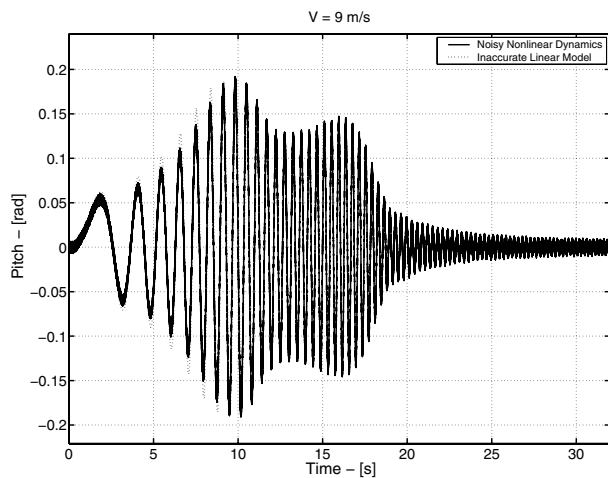
pitch stiffness parameter $k_\alpha = 2.16$ Nm/rad. Hammerstein models are computed to represent these differences at various values of airspeeds. In this way, the estimation process actually identifies the unknown dynamics in the model that account for the differences between measured and predicted responses.

Responses are computed at airspeeds ranging from $V_0 = 5$ to 12 m/s; hence, a total of 8 responses at stable and safe test points are computed. The pitch angle in response to the chirp command is shown in Fig. 9 for the selected airspeed of $V_0 = 12$ m/s.

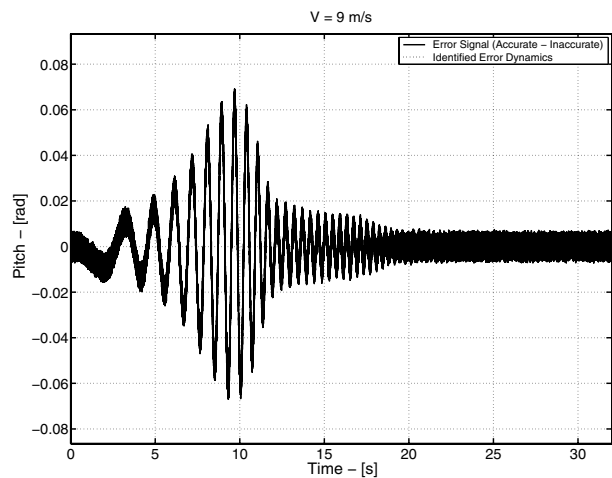
Figure 9a shows the measured linear dynamic \bar{y}_k (solid line) together with the response of the inaccurate linear model y_k (dotted line). The model response differs in both magnitude and period of oscillation from the true response.

By assuming a linear representation for the static map $[\gamma_{12}(\alpha) = 1]$, the Hammerstein model identification algorithm described in Sec. II.B is used to estimate the linear dynamic operator $G_X(V_{12})$ for the unknown dynamics e_k . The dotted line in Fig. 9b shows the time trace of the identified \hat{e}_k signal. Clearly, a good agreement between e_k and \hat{e}_k is obtained, because it is almost impossible to distinguish one from the other.

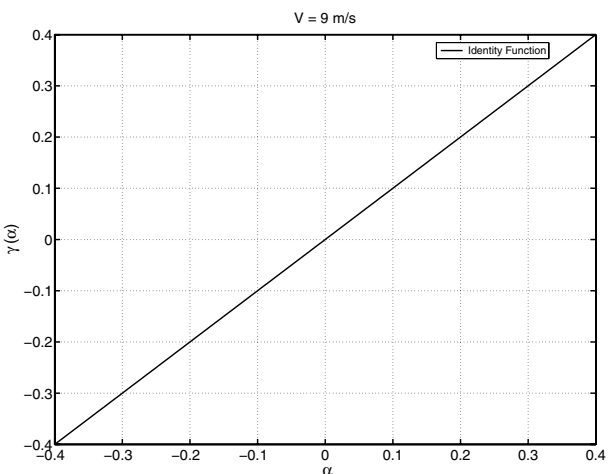
Figure 9c present the time trace of the simulated pitch response \bar{y}_k (solid line) and the output from the updated model $y_k + \hat{e}_k$ (dotted line). Note that in addition to the inaccurate linear model used to generate the basis function set $\{B_k(q)\}_{k=0}^3$, the block-oriented identification approach is capable of accurately reproducing the actual dynamic behavior \bar{y}_k .



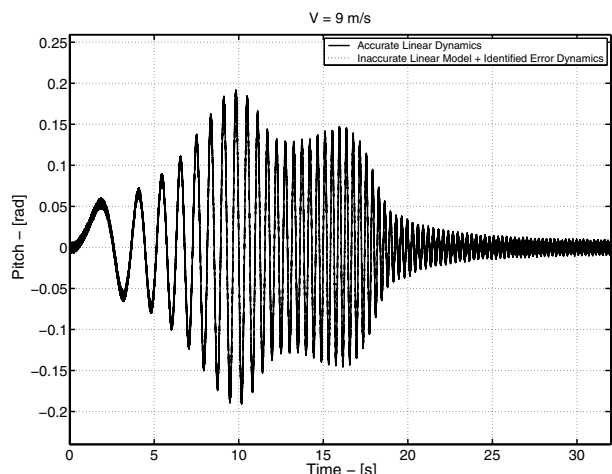
a) Nonlinear dynamics response \bar{y}_k and inaccurate linear model y_k



b) Measured unknown dynamics e_k and estimated unknown dynamics \hat{e}_k

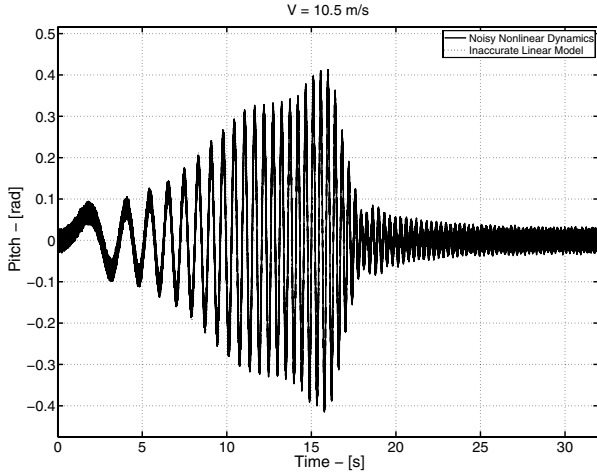
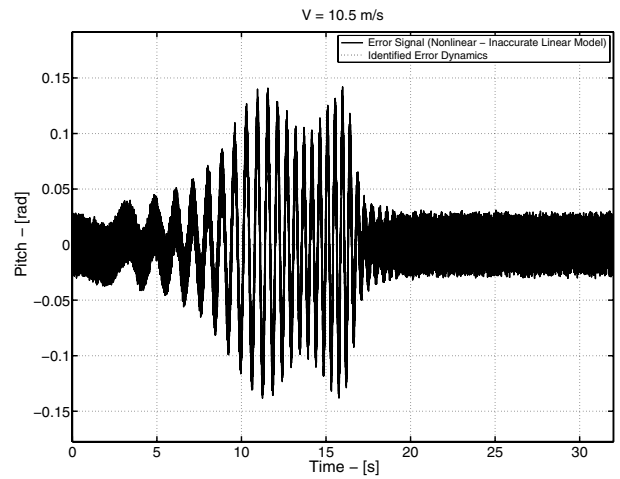
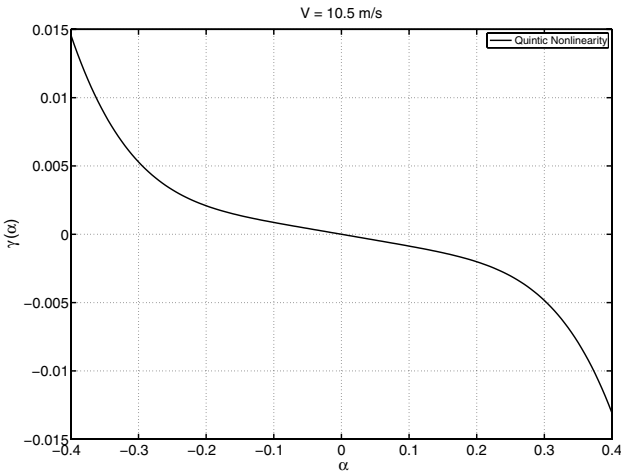


c) Identified linear static map

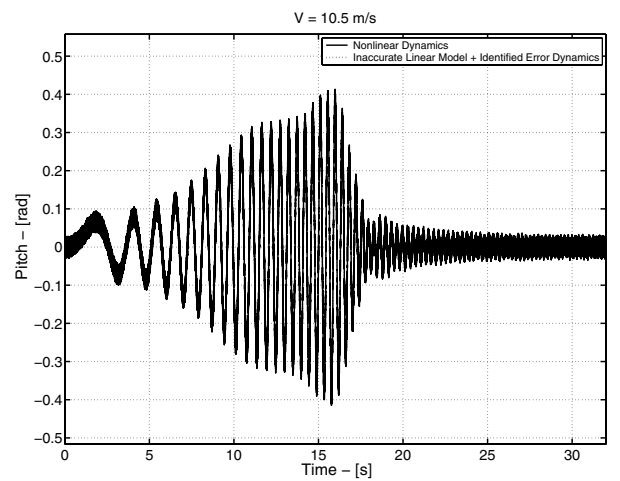


d) Nonlinear dynamics response \bar{y}_k and updated model response $y_k + \hat{e}_k$

Fig. 10 Measured and simulated pitch angle response to a chirp input at $V_0 = 9$ m/s.

a) Nonlinear dynamics response \bar{y}_k and inaccurate linear model y_k b) Measured unknown dynamics e_k and estimated unknown dynamics \hat{e}_k 

c) Identified quintic nonlinearity

d) Nonlinear dynamics response \bar{y}_k and updated model response $y_k + \hat{e}_k$ Fig. 11 Measured and simulated pitch angle response to a chirp input at $V_0 = 10.5$ m/s.

Following Sec. II.C, a parameter-varying (airspeed-dependent) model $X_i^H(\delta_V^i) = G_X^i$ for the unknown dynamics e_k is computed using waypoint data collected up to V_0 ; that is, $X_{10}^H(\delta_V^{10})$ will account for data collected from V_5 until V_{10} , inclusive. In other words, the parameter-varying models are formulated to accurately predict the unknown dynamics at any airspeed higher than V_0 .

The flutter boundary is solved by combining the linear elements P and $G_X(V_0)$ [included in $X_i^H(\delta_V^i)$] using suitable LFT algebra, and the nominal aeroelastic model to be included in Eq. (13) for this linear case is defined as R_i . The speeds at which flutter is predicted to occur are shown in Table 3.

The initial available model at $V_0 = 5$ m/s and $F_u[P, \delta_V^i]$ predicts a flutter speed higher than the true dynamics, with about 2.29% error. The achieved flutter-frequency error is in defect for nearly -1.12% . Clearly, this model does not include any unknown dynamics operator, and the flutter parameters are computed by finding the smallest perturbation δ_V^i that renders unstable the least damped eigenvalue of the state matrix A_p of Eq. (18).

Because of the quadratic matrix polynomial function of the airspeed defined by Eq. (10), the unknown dynamics operators are valid from $V_0 \geq 7$ m/s. It is observed that as the amount of recorded waypoint data used to estimate the unknown dynamics operator is increased, the flutter/LCO framework is able to accurately predict flutter very close to the actual flutter speed. For example, at $V_0 = 11$ m/s, the operator $F_u[R_{11}, \delta_V^i]$ is able to predict both the flutter speed and frequency parameters within 0.9% of their true values.

C. Nonlinear Prediction Case: LCO

Noisy responses are generated at airspeeds ranging from $V_0 = 5$ to 10.5 m/s, providing a set of 7 stable and safe waypoint conditions. As expected, the presence of the strong colored noise in the output signal will mask the weakly embedded nonlinearity up to an airspeed of $V_0 = 9$ m/s. Therefore, a blended identification scenario was considered to be necessary to implement.

For waypoints with the airspeed parameter ranging between $V_0 = 7$ to 9 m/s, a linear static map was recovered, whereas for the remnant test points, a nonlinear static map was estimated. Figures 10a and 11a show the noisy nonlinear dynamics \bar{y}_k (solid line) together with the response of the inaccurate linear model y_k (dotted line). Figures 10b and 11b present the time traces of the identified unknown dynamic \hat{e}_k signals using the blended identification approach. A good agreement is achieved between measurements and predictions, even with the presence of strong colored noise in the output signal \bar{y}_k .

It is observed that a linear static map is sought to be the *best* operator to fit the data with the airspeed parameter ranging between $V_0 = 7$ to 9 m/s (see Fig. 10c). On the contrary, when the airspeed exceeds that threshold value of $V_0 = 10$ m/s, the excitation chirp signal is able to sufficiently excite the nonlinearity (Fig. 11c).

As anticipated, the noise will affect the estimated nonlinearity coefficients, but not the order of the identified polynomials as the nominal airspeed parameter V_0 is changed (i.e., different waypoints). Hence, the identification stage already indicates that a nonlinearity of structural origin has been found. Finally, Figs. 10d and 11d point out

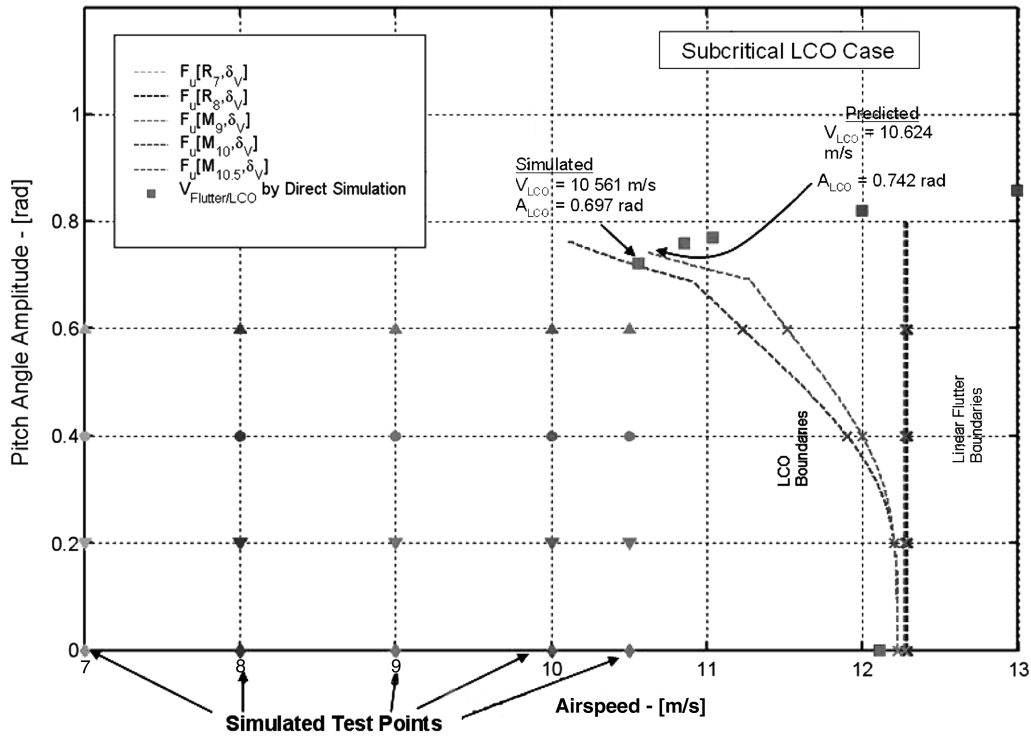


Fig. 12 Simulated and predicted flutter/LCO boundaries.

that noisy pitch responses \bar{y}_k (dotted line) are accurately recovered throughout the updated models $y_k + \hat{e}_k$.

This set of identified Hammerstein models are subsequently used to build the amplitude- and/or airspeed-dependent operators, $X_i^H(\delta_v^i)$ or $X_i^H(a, \delta_v^i)$, that include the parameter-varying model G_X^H for the unknown dynamics e_k . At each airspeed, a parameter-varying model is computed based on a least-squares fit of data collected up to the actual waypoint's airspeed.

Figure 12 shows the linear and nonlinear direct simulation results, together with those of the flutter/LCO predictor tool. It is observed that as the pitch amplitude is varied, the proposed blended identification scenario generates two types of graphs. Vertical lines are related with the identified linear airspeed-dependent operator $X_i^H(\delta_v^i)$, and curved lines are associated with the quasi-linear amplitude- and airspeed-dependent operator $X_i^H(a, \delta_v^i)$.

Along the plot, several markers are used to ease understanding; that is, a diamond, a downward triangle, a circle, and an upward triangle represent a set of discrete amplitude values (namely, $a \triangleq \alpha_0 = \{0, 0.2, 0.4, 0.6\}$). The corresponding values on the flutter/LCO graphs are denoted using an \times .

By replacing the identified static map $\gamma_i(\cdot)$ with its sinusoidal input describing function $N_i(a)$, it allows an implicit parameterization around the amplitude a of the nonlinearity's input signal. For a fixed $N_i(a)$ value, a new linear operator is computed as $M_i = F_i[R_i, N_i(a)]$, and by driving the least damped eigenvalues of M_i to the imaginary axis through the airspeed parameter δ_v^i , the flutter/LCO boundaries in Fig. 12 are traced out.

Table 4 summarizes the most valuable points on the graphs, which are the estimated flutter points associated with linear aeroelastic

instability and the estimated saddle-node or turning points on the subcritical bifurcation diagram. It is observed that as the airspeed is increased and more information is available to generate the parameter-varying models G_X^H included in the linear R_i or quasi-linear M_i operators, the prediction capability of this novel formulation is greatly improved.

A valid question left unanswered until now is when the flight-test engineer will be confident with the flutter/LCO boundaries prediction. Unfortunately, it remains as an open question at this stage of the research. More work is necessary using waypoint data coming from actual flutter envelope-expansion programs to set up some kind of control-room guidelines for the proposed flutter/LCO prediction framework.

A preliminary criteria adopted here was to observe how the predicted saddle-node point was evolving regarding the waypoint's nominal airspeed. If the former is close enough to the latter, then the airspeed interval for the next waypoint is halved. That was the approach followed during the generation of Fig. 12; that is, at $V_0 = 10$ m/s the predicted saddle-node point airspeed is $\hat{V}_{LCO} = 10.112$ m/s, and so the next waypoint airspeed was chosen at $V_0 = (10 + 0.5)$ m/s, giving rise to a saddle-node point airspeed of $\hat{V}_{LCO} = 10.624$ m/s.

Nevertheless, the obtained results are very encouraging considering that we are formulating a control-oriented quasi-linear approach to predict the instability boundary of a complex nonlinear phenomenon.

IV. Conclusions

In contrast to the current state-of-the-art limit-cycle-oscillation (LCO) prediction methodology that employs high-level computational fluid dynamics methods with built-in nonlinear models, the proposed framework blends several well-established control-oriented concepts such as model uncertainty, linear fractional transformation algebra, μ analysis, and block-oriented operator identification. The outcome is an efficient tool capable of identifying, characterizing, and predicting stability margins that reflect both flutter and LCO boundary instabilities.

Based on the presented results, it was found that the underlying model-updating approach has been shown to properly account for

Table 4 Predicted flutter/LCO values summary

Model	Flutter speed, m/s	LCO speed, m/s	LCO amp., rad
True	12.11	10.56	0.69
$F_u[R_7, \delta_v^i]$	12.29	—	—
$F_u[R_8, \delta_v^i]$	12.28	—	—
$F_u[R_9, \delta_v^i]$	12.26	—	—
$F_u[M_{10}, \delta_v^i]$	12.22	10.11	0.76
$F_u[M_{10.5}, \delta_v^i]$	12.22	10.62	0.74

linear errors and unmodeled nonlinearities, as well as to include dependency on the nonlinearity's input amplitude and flight conditions. Clearly, such updated models will provide a substantially improved online prediction capability for flutter/LCO phenomena.

In summary, this paper has showed the following facts:

1) The development of block-oriented models was tuned with the modal dynamics embedded in the experimental data. Specifically, parameter-dependent Hammerstein and Wiener models were devised to characterize the observed nonlinear behavior.

2) The formulation of a novel control-oriented flutter/LCO prediction tool using the data-based amplitude- and airspeed-dependent operators, $\bar{X}_i(\delta_v)$ and/or $\bar{X}_i(a, \delta_v)$, came from the block-oriented identification stage.

3) The application of the control-oriented flutter/LCO framework to a nonlinear aeroelastic pitch-plunge model validated the prediction-engine core algorithms.

Acknowledgments

This work was performed as part of a Phase I Small Business Innovative Research NND05AA44C for NASA Dryden Flight Research Center. The authors thank the anonymous reviewers for their invaluable comments on the draft of this paper. Their suggestions considerably improved the final version of the manuscript.

References

- [1] Buntun, R. W., and Denegri C. M., Jr., "Limit Cycle Oscillation Characteristics of Fighter Aircraft," *Journal of Aircraft*, Vol. 37, No. 5, Sept.–Oct. 2000, pp. 916–918. doi:10.1016/j.jcp.2006.03.038
- [2] Denegri, C. M., Jr., "Limit Cycle Oscillation Flight Test Results of a Fighter with External Stores," *Journal of Aircraft*, Vol. 37, No. 5, Sept.–Oct. 2000, pp. 767–769.
- [3] Dowell E. H., Edwards J., and Strganac T. W., "Nonlinear Aeroelasticity," *Journal of Aircraft*, Vol. 40, No. 5, Sept.–Oct. 2003, pp. 857–874.
- [4] Edwards, J. W., "Transonic Shock Oscillations and Wing Flutter Calculated with an Interactive Boundary Layer Coupling Method," *Euro-mech-Colloquium 349 Simulation of Fluid-Structure Interaction in Aeronautics*, Göttingen, Germany, Sept. 1996.
- [5] Conner, M. D., Tang, D. M., Dowell, E. H., and Virgin, L. N., "Nonlinear Behavior of a Typical Airfoil Section with Control Surface Freeplay: A Numerical and Experimental Study," *Journal of Fluids and Structures*, Vol. 11, No. 1, 1997, pp. 89–109. doi:10.1006/jfls.1996.0068
- [6] Chen, P. C., Sarhaddi, D., and Liu, D. D., "Limit Cycle Oscillation Studies of a Fighter with External Stores," AIAA Paper 98-1727, 1998.
- [7] Brenner, M. J., "Actuator and Aerodynamic Modeling for High-Angle-of-Attack Aeroservoelasticity," AIAA Paper 93-1419, Apr. 1993
- [8] Nayfeh, A. H., and Mook, D. T., "Active Suppression of Aeroelastic System" *AFOSS/AFRL Workshop of Nonlinear Aspects of Aeroelasticity and Related Structural Dynamics*, Mar. 2003.
- [9] Lee, Y. S., Vakakis, A. F., Bergman, L. A., McFarland, D. M., and Kerschen, G., "Triggering Mechanisms of Limit Cycle Oscillations Due to Aeroelastic Instability," *Journal of Fluids and Structures*, Vol. 21, Nos. 5–7, Dec. 2005, pp. 485–529. doi:10.1016/j.jfluidstructs.2005.08.011
- [10] Lind, R., and Brenner, M., "Robust Aeroservoelastic Stability Analysis: Flight Test Applications," *Advances in Industrial Control*, Springer-Verlag, London, 1999, Chaps 7, 9.
- [11] Baldelli, D. H., Lind, R., and Brenner, M., "Robust Aeroelastic Match Point Solutions Using Describing Function Method," *Journal of Aircraft*, Vol. 42, No. 6, Nov.–Dec. 2005, pp. 1596–1604. doi:10.2514/1.11853
- [12] Gómez, J. C., and Baeyens, E., "Identification of Block-Oriented Nonlinear Systems Using Orthonormal Bases," *Journal of Process Control*, Vol. 14, No. 6, 2004, pp. 685–697. doi:10.1016/j.jprocont.2003.09.010
- [13] Baldelli, D. H., Lind, R., and Brenner, M., "Nonlinear Aeroelastic/Aeroservoelastic Modeling Update by Block-Oriented Identification," *Journal of Guidance, Control, and Dynamics*, Vol. 28, No. 5, Sept.–Oct. 2005, pp. 1056–1064. doi:10.2514/1.11792
- [14] Lind, R., Prazenica, R. J., Brenner, M. J., and Baldelli, D. H., "Identifying Parameter-Dependent Volterra Kernels to Predict Aeroelastic Instabilities," *AIAA Journal*, Vol. 43, No. 12, Dec. 2005, pp. 2496–2502.
- [15] Zhou, K., and Doyle, J. C., *Essential of Robust Control*, Prentice–Hall, Upper Saddle River, NJ, 1997, Chap. 9.
- [16] Lind, R., Prazenica, R. J., and Brenner, M. J., "Estimating Nonlinearity Using Volterra Kernels in Feedback with Linear Models," 44th AIAA/ASME/ASCE/AHS Structures, Structural Dynamics, and Materials Conference, Norfolk, VA, AIAA Paper 2003-1406, Apr. 2003.
- [17] Roger, K. L., "Airplane Math Modeling and Active Aeroelastic Control Design," *Structural Aspects of Active Controls* CP-228, AGARD, Neuilly sur Seine, France, 1977, pp. 4.1–4.11.
- [18] Karpel, M., "Design for Active Flutter Suppression and Gust Load Alleviation Using State-Space Aeroelastic Modeling," *Journal of Aircraft*, Vol. 19, No. 3, Mar. 1982, pp. 221–227. doi:10.2514/3.57379
- [19] ZAERO, Software Package, Ver. 8.2, ZONA Technology Inc., Scottsdale, AZ, Mar. 2008.
- [20] Narendra, K. S., and Gallman, P. G., "An Iterative Method for the Identification of Nonlinear Systems Using a Hammerstein Model," *IEEE Transactions on Automatic Control*, Vol. 11, No. 3, 1966, pp. 546–550. doi:10.1109/TAC.1966.1098387
- [21] Wigren, T., "Recursive Prediction Error Identification Using the Nonlinear Wiener Model," *Automatica*, Vol. 29, No. 4, 1993, pp. 1011–1025. doi:10.1016/0005-1098(93)90103-Z
- [22] Zhu, Y., "Identification of Hammerstein Models for Control Using ASYM," *International Journal of Control*, Vol. 73, No 18, 2000, pp. 1692–1702. doi:10.1080/00207170050201771
- [23] Heuberger, P. S. C., Van den Hof, P. M. J., and Wahlberg, W., *Modelling and Identification with Rational Orthogonal Basis Functions*, Springer–Verlag, London, 2005, Chap. 2.
- [24] Gelb, A., and Vander Velde, W. E., *Multiple-Input Describing Functions and Nonlinear System Design*, McGraw–Hill, New York, 1968, Chaps. 1 and 2.
- [25] Ferreres, G., and Fromion, V., "Nonlinear Analysis in the Presence of Parametric Uncertainties," *International Journal of Control*, Vol. 69, No. 5, 1998, pp. 695–716. doi:10.1080/002071798222631
- [26] Doll, C., Ferreres, G., and Magni, J.-F., "μ Tools for Flight Control Robustness Assessment," *Aerospace Science and Technology*, Vol. 3, No. 3, 1999, pp. 177–189. doi:10.1016/S1270-9638(99)80041-8
- [27] Ko, J., Kurdila, A. J., and Strganac, T. W., "Nonlinear Control of a Prototypical Wing Section with Torsional Nonlinearity," *Journal of Guidance, Control, and Dynamics*, Vol. 20, No. 6, Nov.–Dec. 1997, pp. 1181–1189.
- [28] Simulink, Software Package, Ver. 7.0, The MathWorks, Natick, MA, Sept. 2007.